www.MaterialsViews.com

ADVANCED ENERGY MATERIALS
www.advenergymat.de

Extremely Durable High-Rate Capability of a $LiNi_{0.4}Mn_{0.4}Co_{0.2}O_2$ Cathode Enabled with Single-Walled Carbon Nanotubes

*Chunmei Ban, Zheng li, Zhuangchun Wu, Melanie J. Kirkham, Le Chen, Yoon Seok Jung, E. Andrew Payzant, Yanfa Yan, M. Stanley Whittingham, and Anne C. Dillon**

Extensive studies on intercalation electrodes have enabled rapid development of lithium-ion batteries for electronic applications. However, limited cycle life and moderate rate-capability as well as the high-cost of electrode materials still restrict penetration of Li-ion cells for vehicular applications.[1] $LiCoO_2$, the most commonly employed cathode in portable electronics with a capacity of ~135 mAh g^{-1}, is expensive, toxic and unstable at higher voltages (>4.3 V).[2–4] Recently, Ni and Mn substituted compounds ($LiNi_yMn_yCo_{1-2y}O_2$ ($0 < y \leq 0.5$)) have been explored.[2,5–8] Unfortunately, the instability of de-lithiated Li_xNiO_2 and $LiMnO_2$ limits their usage as Li-ion cathodes.[9–11] Although, the $LiNi_yMn_yCo_{1-2y}O_2$ ($0 < y \leq 0.5$) compounds show better thermal stability in organic electrolytes,[12,13] the electronic conductivity and structural stability are lower than that of $LiCoO_2$, thereby negatively affecting rate capability and lifetime, respectively. Different compounds with variations in y ($LiNi_yMn_yCo_{1-2y}O_2$) including the one discussed here have been studied, but it has still not been possible to demonstrate stable high rates with conventional electrodes.[14,15] Recent research in the Whittingham group has shown that $LiNi_yMn_yCo_{1-2y}O_2$ ($y = 0.4, 0.45$) compounds have higher capacities than other compositions but still exhibit low rate-capability.[16]

Many efforts to enhance the conductivity of layered structures that improves the rate performance of Ni and Mn substituted compounds have been undertaken. Carbon coatings have been successfully employed to improve electronic conductivity.[17–19] The use of nanoscale materials is also considered an effective way to ameliorate rate performance due to shorter lithium diffusion paths.[20,21] But, the large surface area of nanomaterials can cause undesirable side reactions that ultimately impair cycling performance.[22] Surface coatings with stable chemicals such as Al_2O_3 and ZrO_2 have been employed to protect the surface resulting in a longer cycle-life.[2,23] However, the electronic conductivity may be reduced if the coating is an insulating material.[24]

In our previous work we demonstrated that single-walled carbon nanotubes (SWNTs) could be employed as a flexible net enabling reversible cycling for a high volume expansion materials.[25] In this work the cathode material does not undergo volume expansion but suffers from poor electrical conductivity and surface over-charge/over-discharge causing capacity fade, especially at high rate. We now demonstrate that the SWNTs can improve both conductivity and also stabilize the surface at an exceptionally high rate of 10C (charge/discharge in 6 min). Specifically, by constructing an $LiNi_{0.4}Mn_{0.4}Co_{0.2}O_2$ cathode (NMCSWNT) with 5 wt.% SWNTs, the cathode is shown to have a capacity of ~130 mAh g^{-1} at 5C and nearly 120 mAh g^{-1} at 10C, both for over 500 cycles. In contrast, the $LiNi_{0.4}Mn_{0.4}Co_{0.2}O_2$ electrode prepared with a conventional method (NMC) without SWNTs has a significantly lower capacity at rates of 5–10C. We also conclusively show with detailed transmission electron microscopy (TEM) as well as Raman and X-ray diffraction (XRD) analysis that this excellent rate capability is due to highly intimate contact between the long crystalline SWNT ropes and the active cathode material. This intimate contact not only enables extraordinary electronic connectivity but also holds the $LiNi_{0.4}Mn_{0.4}Co_{0.2}O_2$ particles to the current collector.

The scanning electron microscopy (SEM) image of the pristine $LiNi_{0.4}Mn_{0.4}Co_{0.2}O_2$ sample in **Figure 1**a shows that the micrometer-sized particles are actually composed of an agglomeration of nanoparticles. The morphology is similar to that reported previously.[13,15] Figure 1b displays the morphology of an NMCSWNT sample containing only 5 wt.% SWNTs. It is clearly evident that the carbon nanotubes infiltrate into the agglomerates so the nanoparticles are interconnected. The intimate contact between the SWNTs and particles is further confirmed with TEM. Figure 1c reveals that a bundle of SWNTs (~8 nm thick) does not simply cross, but rather precisely follows the entire surface of the individual nanoparticles. This suggests a possible chemical interaction between the SWNTs and the particle surface that would not be obtained by simple mixing. Further evidence for this chemical interaction is presented below. In addition to the carbon nanotubes, an amorphous material at the corners of the secondary particles was also observed, as shown in Figure 1d. Based on high-resolution TEM and EDX, the amorphous film consists of an alternative carbon-based material. It is known that the surface of $LiNi_{0.4}Mn_{0.4}Co_{0.2}O_2$

Dr. C. Ban, Dr. Z. Wu, Dr. L. Chen, Y. S. Jung, Dr. Y. Yan, Dr. A. C. Dillon
National Renewable Energy Lab
1617 Cole Boulevard, Golden, CO 80401
E-mail: anne.dillon@nrel.gov
Z. Li, Prof. M. S. Whittingham
Institute for Materials Research
State University of New York at Binghamton
Binghamton, NY, 13902, USA
Dr. M. J. Kirkham, Dr. E. A. Payzant
High-Temperature Materials Laboratory
Oak Ridge National Laboratory
Oak Ridge, TN, 37831

DOI: 10.1002/aenm.201000001

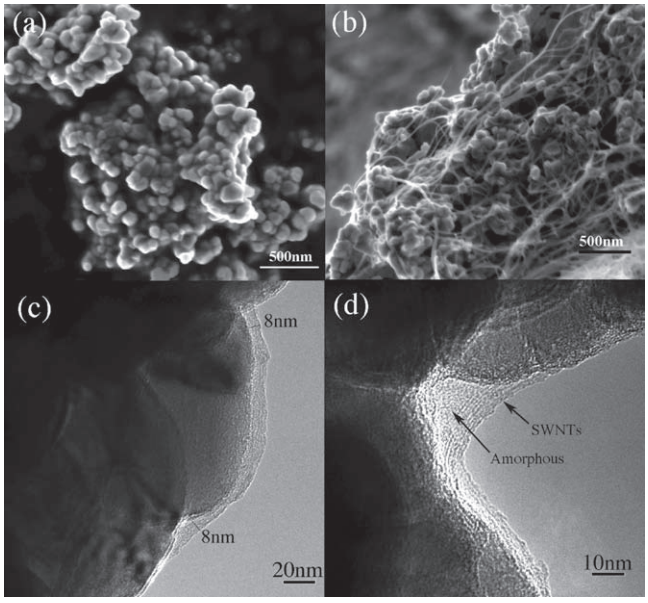

Figure 1. Microscopy images showing various morphologies: a) SEM image of $LiNi_{0.4}Mn_{0.4}Co_{0.2}O_2$ particle agglomerations. b) SEM image of $LiNi_{0.4}Mn_{0.4}Co_{0.2}O_2$ with 5 wt.% SWNT loading (NMCSWNT), revealing that the particles are interconnected with well dispersed SWNTs. c) TEM image of NMCSWNT electrode showing that single-wall carbon nanotubes seamlessly stick on the particle surface. d) TEM image of NMCSWNT electrode showing that the nanotubes also encapsulate an amorphous pocket of Li_2CO_3.

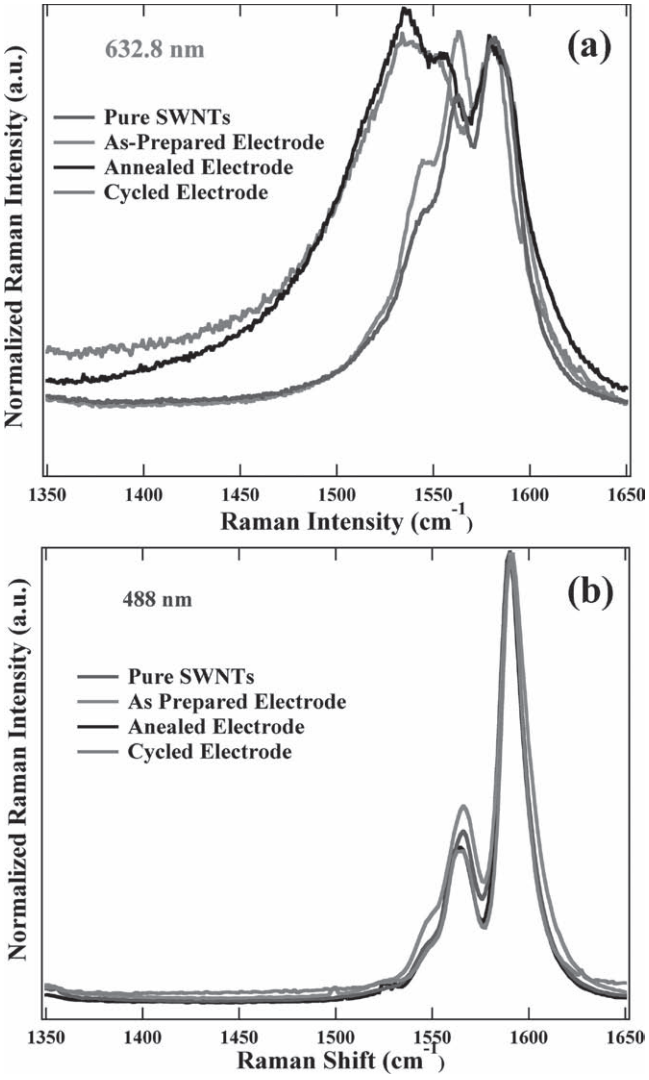

Figure 2. Raman spectra of purified SWNTs, SWNTs during electrode preparation and following annealing as well as following electrochemical cycling of the NMCSWNT cathode for a) excitation at 632.8 nm and b) 488 nm.

easily forms lithium carbonate (Li_2CO_3) due to surface reactivity with H_2O and CO_2.[2,26,27] Although $LiNi_{0.4}Mn_{0.4}Co_{0.2}O_2$ is more stable than $LiNiO_2$, a thicker layer of carbonate may be promoted in our aqueous-based process employed during electrode fabrication. Most of the carbonate films are decomposed during annealing, but the carbonate formed at the corners still exists. In spite of these small pockets of insulating material, the interconnecting nanotubes provide sufficient electronic conductivity that excellent rate capability is achieved as also shown below.

Figure 2 displays the Raman spectra of the purified laser-generated SWNTs employed prior to and during the fabrication and subsequent electrochemical cycling of the NMCSWNT electrode. The Raman spectra of the tangential C-C stretching vibrations are resonantly enhanced bands between 1500–1600 cm^{-1}. Mutiple features are present in Figure 2a, indicating that both metallic and semiconducting tubes are excited at this wavelength of 632.8 nm.[28] The spectra have been normalized to the strongest feature in the pure SWNTs at 1582 cm^{-1}. The slight changes in the relative intensities of the tangential modes may suggest that certain nanotubes have an affinity to the $LiNi_{0.4}Mn_{0.4}Co_{0.2}O_2$ cathode particles, upon processing. Notably, a significant shift in the Raman lines is observed in the electrode after annealing. This indicates that significant charge transfer occurs and that perhaps even a chemical bond is formed. Strong C-C σ bonds in carbon nanotubes ensure structural stability. However, π orbitals, formed by delocalized electrons in carbon nanotubes, enable the possibility of charge-transfer with neighboring $LiNi_{0.4}Mn_{0.4}Co_{0.2}O_2$ particles. We believe that, it is the surface-interaction that further enhances the electronic conductivity of the NMCSWNT electrode.

Figure 2b shows Raman spectra obtained at 488 nm where only semiconducting nanotubes are excited.[29] The peaks have again been normalized to the strongest line in the pure material at 1590 cm^{-1} and again slight changes between the spectrum of the pure tubes and the as-prepared electrode may indicate that certain nanotubes have an affinity to the $LiNi_{0.4}Mn_{0.4}Co_{0.2}O_2$ particles. Interestingly, no shift is observed upon annealing suggesting that the strong charge transfer between the cathode particles and the SWNTs may occur with the metallic nanotubes and/or tubes specifically excited at 632.8 nm. Note that the SWNT signal remains nearly identical after electrochemical cycling for excitation at both 632.8 nm and 488 nm (Figure 2) confirming that the SWNTs are undamaged. Also at this high potential, Li^+ is not intercalated between the nanotubes, which would result in a

quenching of the Raman lines as has been previously observed for SWNTs-incorporated Fe_3O_4 anodes.[25]

The $LiNi_{0.4}Mn_{0.4}Co_{0.2}O_2$ compound has the layered structure of α-$NaFeO_2$ with trigonal symmetry (space group $R\bar{3}m$), which has a close packed oxygen anion sub-lattice with two interstitial cation sites between the close packed layers. In the perfect layered structure, the Li is on one cation site, and the Ni, Mn and Co on the other. However, the structure can transition to a cubic, spinel-type structure in which the cations are mixed between the two sites, with Li in the transition metal layer and the Ni in the Li layer.[5,30] **Figure 3** shows in-situ X-ray diffraction (XRD) patterns of an NMCSWNT electrode during heating and cooling in air between 25 and 525 °C. The peak at around 26 ° is from trace non-nanotube, graphitic carbon impurities in the SWNTs, which diminishes above 300 °C upon oxidation. The broad peak around 22 ° that appears above 300 °C is attributed to crystallization of the well-bundled SWNTs.[31] All of the remaining peaks can be indexed to the α-$NaFeO_2$ structure. The split of the (006)/(102) and (108)/(110) doublets is observed in all of the patterns, which is characteristic of the ordered lamellar structure.[14,15]

Rietveld refinement analysis was performed on the XRD patterns of both $LiNi_{0.4}Mn_{0.4}Co_{0.2}O_2$ (NMC) and $LiNi_{0.4}Mn_{0.4}Co_{0.2}O_2$ with 5 wt.% SWNTs. The lattice parameters of the samples (***a***, ***c***, and ***c/a***) before annealing and after annealing are listed in the **Table 1**. The ratios of ***c/a*** for all of samples are larger than 4.899, which confirms the layered structure.[15,30] (The ***c/a*** ratio is 4.899 for the perfectly mixed, spinel-type structure. Segregation of the Li and transition metals to their respective layers increases the layer spacing, resulting in a larger ***c/a*** ratio.) The lattice parameters of the NMC material without SWNTs maintain the same values before and after annealing in air. However, the lattice parameters of the NMCSWNT material become larger after annealing in air. As we illustrated above, charge-transfer occurs between the SWNTs and the surfaces of $LiNi_{0.4}Mn_{0.4}Co_{0.2}O_2$ particles, instead of simple surface contact. This interaction on the surface of $LiNi_{0.4}Mn_{0.4}Co_{0.2}O_2$ particles may contribute to the observed larger lattice parameters.

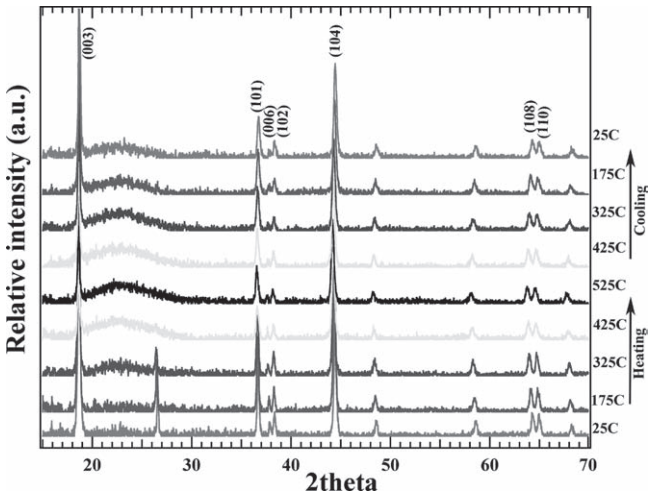

Figure 3. In situ X-ray diffraction patterns of the NMCSWNT electrode following heating from 25 °C to 525 °C and cooling back to 25 °C. All data are collected in air.

Table 1. Refined lattice parameters of $LiNi_{0.4}Mn_{0.4}Co_{0.2}O_2$ and $LiNi_{0.4}Mn_{0.4}Co_{0.2}O_2$–SWNT according to symmetry.

Samples	Preparation cond.	a (Å)	c (Å)	c/a
NMC	As-prepared	2.8693(1)	14.259(2)	4.970(2)
NMC	Annealed in air	2.8696(1)	14.259(1)	4.969(1)
NMCCNT	As-prepared	2.8702(2)	14.254(2)	4.966(1)
NMCCNT	Annealed in air	2.8715(2)	14.271(3)	4.970(3)

Figure 4a exhibits the cyclic voltammetry (CV) plots of the NMCSWNT electrode between 2.5 V and 4.5 V. The curves have one oxidation peak at 3.75 V and one reduction peak at 3.6 V, confirming the perfectly reversible redox reaction between Ni^{2+} and either Ni^{3+} or Ni^{4+}. If cycling occurs at higher voltages, Co^{3+} will also be involved in the reaction and result in a higher capacity. The peaks neither shift nor drop down for 20 cycles. It is the high conductivity of the NMCSWNT electrode that facilitates the electron-transfer during cycling and greatly reduces the polarization. To compare the cycling behavior with conventionally fabricated electrodes, a $LiNi_{0.4}Mn_{0.4}Co_{0.2}O_2$ electrode prepared with binder and conductive additive is also examined here. Both polarization and degradation are observed for the conventional NMC electrode, as shown in the upper inset of Figure 4a. Additionally, an $LiNi_{0.4}Mn_{0.4}Co_{0.2}O_2$ electrode made by simply mixing SWNTs with NMC at room temperature was also tested, as shown in the lower inset of Figure 4a. Besides the degradation observed in the CV, the oxidation peak shifts to a higher voltage in the first de-lithiation process, which is attributed to partially reduced Mn^{4+} ions present after mixing with SWNTs. Thus, large irreversible capacity in the first cycle as well as degradation in cycling performance will therefore occur in the $LiNi_{0.4}Mn_{0.4}Co_{0.2}O_2$ electrode that is simply mixed with SWNTs.

Enhanced electrochemical performance of the NMCSWNT electrode is demonstrated by continuously cycling with variable rates for 100 cycles. Figure 4b displays the charge/discharge capacity *vs.* number of cycles at room temperature. The cells are first cycled at 16 mA g^{-1} (~C/10) and then continuously cycled at 80 mA g^{-1} (~C/2), 320 mA g^{-1} (~2C), 160 mA g^{-1} (~C), 800 mA g^{-1} (~5C), and 80 mA g^{-1} again. The cells are cycled at each rate for 20 cycles. Both the NMC and NMCSWNT cathodes deliver a first charge capacity of 160 mAh g^{-1}, although the NMC cathode has much lower Coulombic efficiency than the NMCSWNT cathode. The higher Coulombic efficiency indicates the stable surface of the NMCSWNT cathode. we note also that the NMCSWNT cathode has a high volumetric capacity of ~200 mAh cm^{-3}. The NMCSWNT cathode shows sustainable capacity at both low and high rates, while the NMC cathode shows a rapid decay in capacity. As shown in the graph, the NMCSWNT cathode has a capacity of ~130 mAh g^{-1} at 5C whilst the NMC cathode has lost all of the initial capacity. Upon returning back to a rate of C/2 after 60 cycles at higher rates, the NMCSWNT cathode delivers the same capacity of 160 mAh g^{-1} while the NMC cathode loses ~50% of its initial capacity. Surface and structural stability play important roles for efficient Li^+ diffusion in the host materials.[2,3] Cell polarization is typical for cathodes materials with poor electronic conductivity. The surface of $LiNi_{0.4}Mn_{0.4}Co_{0.2}O_2$ material with low electronic

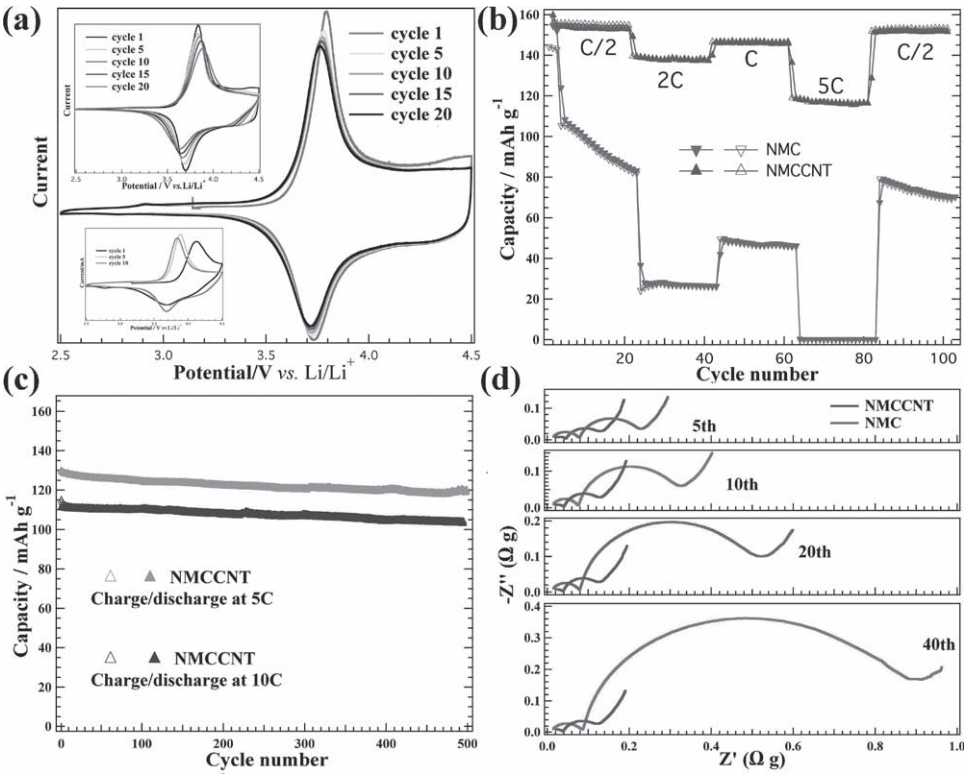

Figure 4. Electrochemical performance for: (a) Cyclic voltammograms (CVs) of NMCSWNT cathode with an inset graph (upper) of CVs for the $LiNi_{0.4}Mn_{0.4}Co_{0.2}O_2$ conventional cathode (NMC); and an insert graph (lower) of CVs for the $LiNi_{0.4}Mn_{0.4}Co_{0.2}O_2$ electrode fabricated by simply mixing in SWNTs. (b) Comparison of NMC cathode and NMCSWNT cathode for one hundred cycles while varying from low to high rates and then returning to low rate. (c): High-rate capability of the NMCSWNT electrode at both 5C and 10C for 500 cycles. (d): Electrochemical impedance spectra (mass-normalized) showing that no surface resistance grows in the NMCSWNT cathode after forty cycles where the NMC cathode reveals rapidly increasing resistance upon cycling.

conductivity is chemically active in the organic electrolyte and evolves oxygen due to overvoltage, which causes performance degradation.[18,32] As we discussed earlier, there is a strong interaction between the SWNTs and the surface of $LiNi_{0.4}Mn_{0.4}Co_{0.2}O_2$ particles, which has greatly improved the conductivity so as to prevent the overcharge and oxygen evolution during cycling. Consequently, extraordinarily improved rate-capability for the NMCSWNT cathode has been demonstrated and is shown in Figure 4c. Here a very stable capacity of ~130 mAh g^{-1} at 5C, and nearly 120 mAh g^{-1} at 10C is observed for 500 cycles. After 500 cycles, the NMCSWNT cathode only loses 8% and 9% of its initial capacity at 5C and 10C, respectively.

The greatly improved electron conductivity has been further verified by impedance spectroscopy. Figure 4d shows Nyquist plots of the NMC and NMCSWNT cathodes. The impedance data are collected after various cycle numbers as labeled in the graph. Z' (Ω g) and –Z" (Ω g) are the magnitude of the real impedance and the imaginary impedance, respectively. The impedance spectra for both NMC and NMCSWNT cathodes are composed of a high-frequency arc, a medium-frequency arc, and a low-frequency Warburg tail. Both high and medium frequency arcs of the NMCSWNT cathode are smaller than that of the NMC cathode. No growth of the medium-frequency semicircle in the NMCSWNT electrode is observed. In contrast, noticeable growth for the NMC electrode is observed indicating increased charge-transfer resistance during cycling.[23] The complete absence of growth of the mid-frequency semicircle for the NMCSWNT electrode, upon cycling, indicates that the $LiNi_{0.4}Mn_{0.4}Co_{0.2}O_2$ surface is conductive and stable. It is the highly conductive and stable surface of the NMCSWNT electrode, which leads to fast ion and electron diffusion, ensuring high-rate durable cycling.

In conclusion, we have demonstrated stable high-rate capability of layered $LiNi_{0.4}Mn_{0.4}Co_{0.2}O_2$ by fabricating an electrode composed of 5 wt.% SWNTs and 95 wt.% $LiNi_{0.4}Mn_{0.4}Co_{0.2}O_2$. Annealing the $LiNi_{0.4}Mn_{0.4}Co_{0.2}O_2$ at 300 °C in air enables the achievement of a layered structure with less cation disorder. Raman spectroscopy suggests that a very strong interaction between the surface of some of the SWNTs and the surface of $LiNi_{0.4}Mn_{0.4}Co_{0.2}O_2$ exists. This may explain why nanotubes uniformly follow the curvature of the particles. This strong surface connectivity ensures the fast diffusion of ions and electrons during cycling, resulting in a sustainable capacity at high rates for 500 hundred cycles.

Experimental Section

The $LiNi_{0.4}Mn_{0.4}Co_{0.2}O_2$ sample was prepared by the mixed hydroxide method, followed by high temperature solid-state heating. The detailed synthesis has been published elsewhere.[14,15] Raw material containing

SWNTs produced by the laser vaporization method were purified by an HNO_3 reflux/air oxidation procedure.[33]

$LiNi_{0.4}Mn_{0.4}Co_{0.2}O_2$ (95 wt.%) and SWNTs (5 wt.%) were mixed and suspended in deionized water by using a 1% concentration of sodium dodecyl sulfate as the surfactant. A film was then fabricated by vacuum filtration. The resulting film was rinsed with deionized water before transferring to the Al foil employed as the current collector. The $LiNi_{0.4}Mn_{0.4}Co_{0.2}O_2$-SWNT electrode was then baked in air at 300 °C prior to electrochemical testing. The conventional $LiNi_{0.4}Mn_{0.4}Co_{0.2}O_2$ electrode (NMC) was made by mixing $LiNi_{0.4}Mn_{0.4}Co_{0.2}O_2$ with acetylene black (Super P, from TIMCAL) and polyvinylidene fluoride (HSV 900, from Kynar) with a weight ratio of 80:10:10 in 1-methyl-2-pyrrolidinone solvent. The slurry was laminated on aluminum foil and air-dried at 110 °C for 6 h before vacuum drying at 120 °C for 8 h. 2025 coin cells were used to characterize the electrochemical properties. In order to compare the electrochemical performance of NMCSWNT electrodes with NMC electrodes, both electrodes were prepared with similar thicknesses of 25–35μm and similar loadings of active material. This was also true for the electrode prepared by simply mixing the SWNTs with NMC. All of the cells were assembled in an argon-filled dry box with Li metal as the negative electrode. A Celgard separator 2325 and 1 M $LiPF_6$ electrolyte solution in 1:1 w/w ethylene carbonate: diethyl carbonate (purchased from Novolyte) were used to fabricate the coin cells. Computer controlled VMP3 channels (BioLogic Science Instruments) were used to carry out electrochemical measurements and electrochemical impedance spectroscopy (EIS). All of the EIS data were collected after fully charging the cells to 4.2 V and holding at 4.2 V for 6 h, with a 5 mV AC signal ranging from 10mHz to 100 kHz.

Both scanning electron microscopy and transmission electron microscopy were utilized to examine the morphology and surface contact between the active material particles and the SWNTs. In-situ X-ray diffraction data with both increasing and decreasing temperature were collected on a Panalytical X'Pert Pro MPD with Cu Kα radiation and an Anton Paar XRK900 hot stage in the High Temperature Materials Laboratory. Data were collected over a 2θ range of 15 to 70 °, with 0.0167 °/step and 90s/step. Scans were collected every 50 ° on heating from 25 to 525 °C and on cooling back to 25 °C for the NMCCNT sample, and at 25, 125, 225, 325, 375, 425 and 25 °C for the NMC sample. The sample height was aligned before each cycle. Raman spectroscopy was performed using both 632.8 nm (HeNe) and 488 nm (Ar-ion) laser excitation. The back-scattered light was analyzed with a Jobin Yvon 270M spectrometer equipped with a liquid-nitrogen-cooled Spectrum One charge-coupled device (CCD) and holographic notch filters. Averaging three 30 s scans was sufficient to obtain high intensity, well-resolved Raman spectra.

Acknowledgements

The U.S. Department of Energy (DOE) under contract No. DE-AC36–08GO28308, DE-AC02–05CH11231, and the Batteries for Advanced Transportation Technologies (BATT) Program funded this work at NREL and at Binghamton, under contract No. 6807148. The in-situ XRD research during heating and cooling was done in the Oak Ridge National Laboratory's High Temperature Materials Laboratory User Program, which is sponsored by the U.S. Department of Energy, EERE, Vehicle Technologies Program.

Received: October 21, 2010
Revised: November 24, 2010
Published online: December 15, 2010

[1] a) H. Yang, S. Amiruddin, H. J. Bang, Y. K. Sun, J. Prakash, *J. Ind. Eng. Chem.* **2006**, *12*, 12; b) Basic Research Needs for Electrical Energy Storage, U.S. Department of Energy, Washington, DC, USA, 2007. Available from http://www.sc.dog.gov/bes/reports/files/EES_rpt.pdf.
[2] M. S. Whittingham, *Chem. Rev.* **2004**, *104*, 4271.
[3] J. M. Tarascon, M. Armand, *Nature* **2001**, *414*, 359.
[4] N. A. Chernova, M. Roppolo, A. C. Dillon, M. S. Whittingham, *J. Mater. Chem.* **2009**, *19*, 2526.
[5] T. Ohzuku, Y. Makimura, *Chem. Lett.* **2001**, 642.
[6] K. M. Shaju, G. V. S. Rao, B. V. R. Chowdari, *Electrochim. Acta* **2002**, *48*, 145.
[7] I. Belharouak, Y. K. Sun, J. Liu, K. Amine, *J. Power Sources* **2003**, *123*, 247.
[8] Z. H. Lu, D. D. MacNeil, J. R. Dahn, *Electrochem. Solid-State Lett.* **2001**, *4*, A200.
[9] B. Ammundsen, J. Paulsen, *Adv. Mater.* **2001**, *13*, 943.
[10] G. Vitins, K. West, *J. Electrochem. Soc.* **1997**, *144*, 2587.
[11] J. R. Dahn, E. W. Fuller, M. Obrovac, U. Vonsacken, *Solid State Ionics.* **1994**, *69*, 265.
[12] D. D. MacNeil, Z. Lu, J. R. Dahn, *J. Electrochem. Soc.* **2002**, *149*, A1332.
[13] S. Jouanneau, D. D. MacNeil, Z. Lu, S. D. Beattie, G. Murphy, J. R. Dahn, *J. Electrochem. Soc.* **2003**, *150*, A1299.
[14] J. K. Ngala, N. A. Chernova, M. M. Ma, M. Mamak, P. Y. Zavalij, M. S. Whittingham, *J. Mater. Chem.* **2004**, *14*, 214.
[15] M. M. Ma, N. A. Chernova, B. H. Toby, P. Y. Zavalij, M. S. Whittingham, *J. Power Sources* **2007**, *165*, 517.
[16] Z. Li, N. Chernova, M. Roppolo, S. Upreti, M. S. Whittingham, in 2009 *MRS Fall Meeting*, Boston, MA **2009**.
[17] Z. H. Chen, J. R. Dahn, *J. Electrochem. Soc.* **2002**, *149*, A1184.
[18] B. L. Cushing, J. B. Goodenough, *Solid State Sci.* **2002**, *4*, 1487.
[19] J. Liu, Q. Y. Wang, B. Reeja-Jayan, A. Manthiram, *Electrochem. Commun.* **2010**, *12*, 750.
[20] C. M. Ban, N. A. Chernova, M. S. Whittingham, *Electrochem. Commun.* **2009**, *11*, 522.
[21] J. Jamnik, J. Maier, *Phys. Chem. Chem. Phys.* **2003**, *5*, 5215.
[22] A. S. Arico, P. Bruce, B. Scrosati, J. M. Tarascon, W. Van Schalkwijk, *Nat. Mater.* **2005**, *4*, 366.
[23] Y. S. Jung, A. S. Cavanagh, A. C. Dillon, M. D. Groner, S. M. George, S. H. Lee, *J. Electrochem. Soc.* **2010**, *157*, A75.
[24] Y. S. Jung, A. S. Cavanagh, L. A. Riley, S. H. Kang, A. C. Dillon, M. D. Groner, S. M. George, S. H. Lee, *Adv. Mater.* **2010**, *22*, 2172.
[25] C. M. Ban, Z. C. Wu, D. T. Gillaspie, L. Chen, Y. F. Yan, J. L. Blackburn, A. C. Dillon, *Adv. Mater.* **2010**, *22*, E145.
[26] N. Mijung, Y. Lee, J. Cho, *J. Electrochem. Soc.* **2006**, *153*, A935.
[27] J. Li, J. M. Zheng, Y. Yang, *J. Electrochem. Soc.* **2007**, *154*, A427.
[28] A. C. Dillon, M. Yudasaka, M. S. Dresselhaus, *J. Nanosci. Nanotechnol.* **2004**, *4*, 691.
[29] A. C. Dillon, P. A. Parilla, J. L. Alleman, T. Gennett, K. M. Jones, M. J. Heben, *Chem. Phys. Lett.* **2005**, *401*, 522.
[30] S. Gopukumar, K. Y. Chung, K. B. Kim, *Electrochim. Acta* **2004**, *49*, 803.
[31] J. L. Blackburn, Y. Yan, C. Engtrakul, P. A. Parilla, K. Jones, T. Gennett, A. C. Dillon, M. J. Heben, *Chem. Mat.* **2006**, *18*, 2558.
[32] D. Aurbach, K. Gamolsky, B. Markovsky, G. Salitra, Y. Gofer, U. Heider, R. Oesten, M. Schmidt, *J. Electrochem. Soc.* **2000**, *147*, 1322.
[33] A. C. Dillon, T. Gennett, K. M. Jones, J. L. Alleman, P. A. Parilla, M. J. Heben, *Adv. Mater.* **1999**, *11*, 1354.